Neuropharmacology 177 (2020) 108160

Contents lists available at ScienceDirect

Neuropharmacology

journal homepage: www.elsevier.com/locate/neuropharm

Progression of obsessive compulsive disorder-like grooming in Sapap3 knockout mice: A longitudinal [^{11}C]ABP688 PET study

Dorien Glorie[a], Jeroen Verhaeghe[a], Alan Miranda[a], Istvan Kertesz[a,b], Leonie wyffels[a,b], Sigrid Stroobants[a,b], Steven Staelens[a,*]

[a] Molecular Imaging Center Antwerp (MICA), University of Antwerp, Wilrijk, Belgium
[b] Department of Nuclear Medicine, Antwerp University Hospital, Edegem, Belgium

HIGHLIGHTS

- mGluR5 availability declines in OCD relevant brain regions of Sapap3 ko mice.
- The grooming frequency in Sapap3 ko mice is already increased at age 3 months.
- [^{11}C]ABP688 PET can be applied to monitor disease progression in Sapap3 ko mice.

ARTICLE INFO

Keywords:
Obsessive compulsive disorder (OCD)
PET
Metabotropic glutamate receptor 5 (mGluR5)
SAP90/PSD-95 associated protein 3 (Sapap3)
Mouse model
Grooming behavior

ABSTRACT

We aimed to evaluate [3-(6-methyl-pyridin-2-ylethynyl)-cyclohex-2-enone-0-^{11}C-methyloxime] ([^{11}C]ABP688) small animal positron emission tomography (μPET) as a biomarker to visualize possible longitudinal changes in metabotropic glutamate receptor 5 (mGluR5) availability in the brain of SAP90/PSD-95 associated protein 3 (Sapap3) knockout (ko) mice, showing obsessive compulsive disorder (OCD)-like behavior.

Methods: Alongside the assessment of grooming, we performed [^{11}C]ABP688 μPET/CT imaging in wildtype (wt; n = 10) and ko (n = 11) mice both at 3 and 9 months. Using the simplified reference tissue method (SRTM), the nondisplaceable binding potential (BP_{ND}) was calculated representing the *in vivo* availability of the metabotropic glutamate receptor 5 (mGluR5) in the brain with the cerebellum as a reference region. Longitudinal voxel-based statistical parametric mapping (SPM) was performed on BP_{ND} images. Results were verified using [^{11}C]ABP688 *ex vivo* autoradiography, [^{3}H]ABP688 *in vitro* autoradiography, and mGluR5 immunohistochemistry.

Results: Cross-sectional comparisons revealed significantly increased grooming parameters in ko animals, at both time points. A significant longitudinal increase in % grooming duration (+268.25%; $p < 0.05$) reflected aggravation of this behavior in ko mice. [^{11}C]ABP688 μPET revealed significantly lower mGluR5 availability in the cortex, striatum, hippocampus, and amygdala of ko mice at both ages. A significant longitudinal BP_{ND} decline was present for ko mice ($p < 0.01$: cortex −17.14%, striatum −19.82%, amygdala −23.57%; $p < 0.05$: hippocampus −15.53%), which was confirmed by SPM ($p < 0.01$).

Conclusion: Sapap3 ko mice show a decline in mGluR5 availability in OCD relevant brain regions parallel to the worsening of OCD-like behavior. This demonstrates a potential role for [^{11}C]ABP688 PET as a biomarker to monitor disease progression *in vivo*.

1. Introduction

Obsessive compulsive disorder (OCD) is a neuropsychiatric disease with a lifetime prevalence of 1–3% (Ruscio et al., 2010) and is usually characterized by a chronic course. Patients are preoccupied with recurrent, intrusive obsessions and/or time-consuming, repetitive compulsions to reduce distress associated with these obsessions or with self-imposed rigid rules (Abramowitz et al., 2009). Consequently, daily functioning is drastically impaired, reflected by the ranking of this disease in the top 10 causes of illness-related disability based on quality of life and lost earnings by the World Health Organization (Murray and Lopez, 1996). This disorder remains underdiagnosed and when treated, a substantial group of patients remains refractory (Denys et al., 2010). Both clinical and preclinical studies already pinpointed a role for a

* Corresponding author. Molecular Imaging Center Antwerp (MICA), University of Antwerp, Universiteitsplein 1, Wilrijk, Belgium.
E-mail address: steven.staelens@uantwerpen.be (S. Staelens).

https://doi.org/10.1016/j.neuropharm.2020.108160
Received 26 August 2019; Received in revised form 18 March 2020; Accepted 21 May 2020
Available online 23 May 2020

dysfunctional corticostriatothalamocortical (CSTC) circuit (Graybiel and Rauch, 2000; Pauls et al., 2014; Ting and Feng, 2011), which is involved in the integration and selection of motor and cognitive programs and their downstream implementation. Unfortunately, current clinical OCD research is hampered to test for causality and is associated with certain limitations such as patient heterogeneity, comorbidities, and medication history. Consequently, underlying molecular mechanisms remain elusive, causing delay in the identification of improved therapy paradigms.

Research animal models may function as a valuable tool to study the mechanisms underlying OCD-like behavior, thereby contributing to scientific progress. Mice display a set of behaviors with relevance to OCD when lacking the SAP90/PSD-95 associated protein (Sapap3; DLGAP3; GKAP3) (Welch et al., 2007), thereby covering the face validity of this model. This protein belongs to the group scaffolding proteins that functionally links different types of glutamate receptors at the level of the postsynaptic density (O'Connor et al., 2014). These mice show excessive pathological grooming, increased anxiety-like behavior, and an imbalanced striatal output (Ade et al., 2016). In addition, this model's predictive validity is supported by the alleviation of compulsive-like grooming and anxiety-like behavior after chronic fluoxetine administration (Welch et al., 2007), which is the current first-line treatment for patients. In addition, deep-brain stimulation (a last-resort treatment for refractory patients) of the internal capsule and dorsal ventral striatum reduced pathological grooming in Sapap3 ko mice (Pinhal, 2018). Also, selective re-expression of Sapap3 in the striatum, a core structure in the dysfunctional CSTC circuit in patients, reversed OCD-like phenotypes (Welch et al., 2007; Mahgoub et al., 2016). A recent study in postmortem tissue samples of OCD patients reported a signficantly decreased Sapap3 expression in cortical and striatal regions (Piantadosi et al., 2019). Genetic studies provide moderate support concerning construct validity (Bienvenu et al., 2009; Stewart et al., 2013; Züchner et al., 2009).

Previous work in this model identified overactivation of the G-protein coupled metabotropic glutamate receptors (mGluRs) 5 in corticostriatal connections as a driver of OCD-relevant phenotypes in Sapap3 ko mice (Ade et al., 2016). This excessive mGluR5 signaling was characterized by constitutive activation in absence of its orthosteric ligand glutamate. Negative allosteric modulation of this receptor corrected pathological grooming (Ade et al., 2016). These facts imply a potential role for glutamate modulators in OCD treatment. Here, we use small-animal positron emission tomography (μPET) to explore whether [3-(6-methyl-pyridin-2-ylethynyl)-cyclohex-2-enone-0-^{11}C-methyloxime] ([^{11}C]ABP688), a radiolabeled mGluR5 negative allosteric modulator (Ametamey et al., 2006), is a possible molecular biomarker to visualize this phenomenon *in vivo*. We seek to investigate whether aggravation of the grooming phenotype parallels changes in mGluR5 availability via longitudinal μPET measurements. To date, no molecular imaging studies (μPET) were carried out in genetic models with OCD-relevant phenotypes and no previous studies characterized grooming behavior in Sapap3 ko mice longitudinally.

2. Material and methods

2.1. Animals

For the longitudinal μPET experiment, female Sapap3$^{-/-}$ ko mice (n = 11) were bred in-house from heterozygous Sapap3$^{+/-}$ breeder pairs (kindly obtained from Prof. Dr. G. Feng, Massachusetts Institute of Technology) at the University of Antwerp. Genotypes were determined via PCR of mouse ear DNA. All Sapap3$^{-/-}$ ko mice (n = 11) and age-matched wildtype (wt) C57BL/6J mice (n = 11) were co-housed in individually ventilated cages under controlled conditions (12h normal light–dark cycles, 20–23°C, and 50–55% relative humidity) with water and rodent food pellets *ad libitum*. Additional female satellite animals (age 3 months n = 5/genotype) for [^{3}H]ABP688 *in vitro* autoradiography were kept under the same circumstances. All animal procedures were performed in accordance with the European Ethics Committee (decree 86/609/CEE). The study protocol was approved by the Animal Experimental Ethical Committee of the University of Antwerp, Antwerp, Belgium.

2.2. Behavioral evaluation

Prior to both the [^{11}C]ABP688 μPET scan at the age of 3 and 9 months (mo), each animal was monitored by video recording to assess grooming behavior. The recordings were performed during the dark cycle (08.00 p.m.–08.00 a.m.) in the PhenoTyper® cage (Noldus Information Technology, The Netherlands). A 30-min time window in the middle of the 12h active period (01.45 a.m.–02.15 a.m.) was selected for blind scoring. All recordings were manually scored by two independent observers using open access software (CowLog, Natural Resources Institute, Finland). Grooming included all sequences of face-wiping, scratching/rubbing of head and ears, and full-body grooming (Welch et al., 2007).

2.3. Tracer synthesis

Based on a previous description of the radiosynthesis (Ametamey et al., 2006), [^{11}C]ABP688-E is prepared by reaction of 0.5 mg desmethyl-ABP688 (E/Z) with $^{11}C–CH_3SO_3CF_3$ in 400 μL acetone in the presence of 10 μL 1N NaOH for 4 min at room temperature. For purification, the crude reaction mixture was injected into an analytical HPLC column (WatersXBridge C18, 5 μm, 4.6 × 150 mm) with an eluent of 0.05 M sodium acetate (pH 5.5) and ethanol (55/45, v/v) at a flow rate of 1 mL/min to isolate the [^{11}C]ABP688-E. The purified [^{11}C]ABP688-E is filtrated through a sterile Millipore Millex-GV filter (0.22 μm) and diluted with 0.9% NaCl through the same filter to reduce the ethanol concentration to < 10%. The injected cold mass was kept below 5.00 nmol/kg to avoid cold mass effects (Hume et al., 1998). At the 3 mo timepoint, the mean molar activity (A_m) at time of injection was 62.57 ± 16.99 MBq/nmol for the wt group and 63.42 ± 16.36 MBq/nmol for the ko group. At 9 mo, the mean A_m was 41.97 ± 7.71 MBq/nmol and 39.00 ± 4.80 MBq/nmol, respectively.

2.4. [^{11}C]ABP688 dynamic μPET scans

At the age of 3 and 9 mo all mice were subjected to a dynamic μPET/CT acquisition. Mice were anesthetized using isoflurane (IsoFlo®, Zoetis, USA) mixed with medical oxygen (induction 5%, maintenance 2%) and placed on a heated blanket (37.5°C). A catheter (tubing: P10, Instech Solomon, USA; needle: BD Microlance™ 30G, BD, USA) was placed in the tail vein for later iv bolus administration of the tracer. Afterwards, the animals were positioned on the heated bed of the scanner. Parallel to the start of the 60-min dynamic μPET acquisition, a bolus of [^{11}C]ABP688 was administered using an automated syringe pump at a rate of 1 mL/min (model 11 Elite, Harvard Apparatus, USA). Subsequently, a 10-min 80 kV/500 μA CT scan was acquired for attenuation and scatter correction. Acquisitions (60 + 10 min; frames: 12 × 10s, 3 × 20s, 3 × 30s, 3 × 60s, 3 × 150s and 9 × 300s) were performed on 2 Siemens Inveon μPET/CT scanners (Siemens Preclinical Solutions, USA). During scanning procedures, both the respiratory and heart rate were monitored and body temperature was kept at 37.0°C with a feedback air flow system (Minerve, France). Animal and scan parameters are represented in Table 1.

Table 1
Overview of animal and scan parameters for [^{11}C]ABP688 dynamic μPET scans with an equal injected cold mass for both groups at both timepoints (mo = months; wt = wildtypes; ko = knockouts).

age	genotype	animal number	body weight (g)	Injected radioactivity (Mbq)	injected cold mass (nmol/kg)
3 mo	wt	10	20.98 ± 1.22	7.11 ± 1.73	5.46 ± 0.44
	ko	11	19.79 ± 1.13	6.68 ± 1.74	5.53 ± 0.26
9 mo	wt	8	25.84 ± 1.83	5.60 ± 1.44	5.11 ± 0.38
	ko	11	23.54 ± 1 .77	4.60 ± 0.83	5.00 ± 0.37

2.5. Image processing

For quantitative image analysis, μPET images were reconstructed using two-dimensional ordered subset expectation maximization (2D-OSEM) with four iterations and 16 subsets after Fourier rebinning. The images were reconstructed on a $128 \times 128 \times 159$ grid with a voxel size of $0.776 \times 0.776 \times 0.796$ mm. Normalization, dead time correction, random subtraction, CT-based attenuation and simulated single-scatter corrections, as well as detector response modeling for parallax errors were applied. Reconstructed images were processed in PMOD v3.6 (PMOD Technologies, Switzerland). A static image corresponding to the time-averaged frames of each dynamic acquisition was spatially transformed to a mouse brain [^{11}C]ABP688 PET template (in-house). This PET template (via CT) already corresponded to a standardized MR template space (Waxholm MR) (Johnson et al., 2010) with the corresponding volume-of-interest (VOI) definitions. The obtained matrix from the aforementioned brain normalization step was applied to transform all dynamic scans to that [^{11}C]ABP688 template space. The regional time-activity curves were extracted from the resulting raw non-smoothed images via the superimposition of the VOI template. These extracted time-activity curves served as input for the simplified reference tissue model (SRTM) (Lammertsma and Hume, 1996). This allows quantification of the receptor kinetics via the expression of tracer uptake in these VOI regions compared to uptake in a reference region devoid of the target receptor, but with a similar level of non-displaceable binding. Based on this method (implemented in PMOD software), the regional non-displaceable binding potential (BP_{ND}) was calculated with the cerebellum as a reference region (Verhaeghe et al., 2018). In addition, pixelwise kinetic modeling, using SRTM2 (Wu and Carson, 2002), was applied to generate a parametric BP_{ND} image for each animal. Subsequently, averaged BP_{ND} images were calculated for all groups. For visualization purposes, these images were smoothed using an isotropic Gaussian filter (FWHM = 0.5 mm).

2.6. Ex vivo and in vitro autoradiography

Both *ex vivo* [^{11}C]ABP688 and *in vitro* [^{3}H]ABP688 autoradiography was used to verify the obtained *in vivo* μPET results. *Ex vivo* autoradiography was performed on brain slices of a representative animal per genotype (9 mo old). For this procedure, the μPET protocol was replicated. Again, both anesthetized mice received a bolus of [^{11}C]ABP688 via a tail vein catheter (injected radioactivity: wt: 3.44 MBq, ko: 3.11 Mbq; injected cold mass: wt: 5.25 nmol/kg, ko: 5.23 nmol/kg). After an uptake period of 8 min, animals were sacrificed, brains were rapidly removed and snap frozen in 2-methylbutane (−35°C, 2 min). Serial sagittal brain sections (40 μm) of both animals were collected on Superfrost Plus slides (Thermo Fischer Scientific, USA) using a cryostat (Leica, Germany) with Paxinos and Watson coordinates (4th edition, 2013) as a reference (1.56 mm lateral). Based on the injected radioactivity and the estimated percentage of tracer that potentially reaches the brain, a range of tracer dilutions was prepared to obtain a standard curve (kBq per μL of reference solution, kBq/μL) representative for the amount of tracer present in the brain tissue. Fifty-five minutes after collection of the brain tissue, a phosphor imaging plate (BAS-IP MS, 2040; Fujifilm, Japan) was placed on the air-dried slides together with a range of standard dilutions (2 μL drops on Benchkote) in a light impermeable cassette (Hypercassette, Amersham Biosciences, UK) for a total exposure of 2 h.

In vitro autoradiography was performed using [^{3}H]ABP688 (American Radiolabeled Chemicals Inc, USA), which was synthesized by a reaction of the oxime with methyl iodide [^{3}H] and was purified using HPLC. The molar radioactivity was 80 Ci/mmol and the radiochemical purity was 99%. Brain tissue was collected and immediately snap frozen in 2-methylbutane (−35°C, 2 min, one hemisphere). Again, serial sagittal brain sections (20 μm) were collected on Superfrost Plus slides (Thermo Fischer Scientific, USA) and similarly processed and stored as for *ex vivo* autoradiography. Sections were thawed at room temperature, preincubated for 30 min with binding buffer (50 mM Tris-HCl buffer, pH 7.4, containing 10 mM $MgCl_2$), and dried using an airflow. Per animal (5/genotype age 9 mo: randomly selected from the μPET cohorts and a satellite group of 5/genotype age 3 mo), three sections were incubated with total binding (TB) solution (1 nM of [^{3}H]ABP688 in binding buffer) and three sections with non-specific binding (NB) solution (1 nM of [^{3}H]ABP688 + 5 μM of 3-((2-Methyl-4-thiazolyl)ethynyl)pyridine) (MTEP hydrochloride, Tocris, UK)) for 60 min at room temperature. A third incubation condition with L-glutamate was performed (1 nM of [^{3}H]ABP688 + 5 μM of L-glutamatic acid (Merck, USA)) to check for mGluR5 binding competition. On ice, all sections were washed 3 times in 50 mM Tris-HCl buffer, followed by 5 dips in dH_2O on ice. Sections were air dried at room temperature for 2 h to prepare for exposure on an imaging plate (BAS-IP TR2025 E, Fujifilm, Japan). All sections were exposed for a total duration of 24 h, together with a tritium standard for later quantification (American Radiolabeled Chemicals Inc, USA).

For both approaches, plate reading was carried out using the Typhoon FLA7000 (GE Healthcare, USA) with a pixel size of 25 μm. The obtained digital image was processed using ImageJ software (National Institutes of Health, USA), thereby determining local tissue concentrations in the different regions-of-interest via interpolation of mean gray values on the obtained standard curve. For *ex vivo* autoradiography, twenty slides per region (cortex, striatum, hippocampus) per animal were analyzed. The obtained mean value per region was decay corrected to the time at which the exposure was started and expressed as the % injected radioactivity/mL (%IR/mL). Concerning the *in vitro* approach, three sections per region (cortex, striatum, hippocampus) per animal were analyzed. Here, we report the obtained mean value per region in nCi/mg.

2.7. mGluR5 immunohistochemistry

Nine-mo old mice were sacrificed followed by the rapid collection of brain tissue. One hemisphere was snap frozen in 2-methylbutane (−35°C, 2 min) for *ex vivo* autoradiography. For mGluR5 immunohistochemistry (IHC) the other hemisphere was put into 4% paraformaldehyde overnight. The tissue was processed using the Exelsior ES (Thermo Fisher Scientific, USA), and was paraffine embedded on a routine base. Using a microtome (HM340E, Thermo Fisher Scientific, USA), serial sagittal sections of 5 μm were collected Superfrost Plus Slides (Thermo Fisher Scientific, USA) 1.56 mm lateral from the interaural line (Paxinos and Watson, 4th Edition, 2013) to include the cortex, the striatum and the hippocampus in one section. For the

mGluR5 staining, three section per animal were stained. The tissue slides were first rehydrated using: 2×5 min xylene; 2×5 min 100%; 1×5 min 96% ethanol; 1×5 min 80%; 1×5 min dH_2O. For antigen unmasking, the slides were submerged for 10 min in 10 mM citrate buffer pH 6.0 (+ a 30 min cooldown in buffer). After a rinse in PBS, the slides were incubated with 3% H_2O_2 during 5 min to quench endogenous peroxidases. Then, the slides were rinsed with 0.03% Triton X-100 in PBS (2×5 min) and incubated with 10% normal horse serum (NHS) in PBS for 1 h. Subsequently, the sections were incubated overnight at room temperature with a primary polyclonal antibody solution of rabbit anti-mGluR5 (1:250, AB5675, Merck Millipore, USA) in blocking buffer (5% NHS). Again, the slides were washed with 0.03% Triton X-100 in PBS (2×5 min) and PBS (5 min) follow by a 1-h incubation with the peroxidase-conjugated goat anti-rabbit secondary antibody (1:500, Jackson ImmunoResearch, UK) in blocking buffer (5% NHS). Followed by a last rinse in PBS (3×5 min), the sections were exposed to 3,3' diaminobenzidine (DAB, Dako Agilent, USA) for 10 min. Finally, the reaction was stopped with tap water and a coverslip was applied using mounting medium (DPX, Merck Millipore, USA).

All images of the regions-of-interest were taken at a 20× magnification with a Nikon Ti wide-field microscope equipped with a Nikon DS-Fi2 camera using NIS Elements Ar software (Nikon Instruments, France). Image processing was performed using ImageJ software (National Institutes of Health, USA). After a conversion to 8-bit images, an intensity threshold was visually set to exclude the background. A threshold was imposed for each region separately, based on a stack including all the obtained images. The regions-of-interest were manually delineated, blind for the genotype. In addition, the integrity of the tissue was checked for all sections, damaged regions were excluded. The % area stained was extracted from the region-of-interest as the read-out for the amount of stained mGluR5 receptors.

2.8. Data and statistical analysis

All statistical analysis was performed in GraphPad Prism 8 (GraphPad Software, USA). The Shapiro-Wilk test was applied to all grouped data to confirm normality. For statistical analysis, a significance level of $p < 0.05$ was imposed. One wt animal was excluded from the analysis due to an edge artifact at the level of the hippocampus in the reconstructed image.

For behavioral data analysis, grooming bouts were defined to have a duration ≥1s, and sessions separated ≥2s constituted a new bout (Ade et al., 2016). In addition, the 30-min recordings were scored for inactivity defined by the absence of movement for ≥40s (Pack et al., 2007). The total time of inactivity was subtracted from the total recording time for each animal, prior to calculating the % duration grooming. In addition, the obtained grooming frequency was also corrected for inactivity. Based on the outcome of the Shapiro-Wilk test for normality, a Mann-Whitney test was performed to compare behavioral parameters between both groups at one timepoint. The Wilcoxon matched-pairs signed rank test was used to identify longitudinal differences. All behavioral data is expressed as the averaged parameter-of-interest ± standard error (SE) for both wt and ko groups.

VOI-based [^{11}C]ABP688 μPET data passed the normality test. A two-way ANOVA with *post-hoc* Bonferroni correction for multiple comparisons was applied to investigate whether significant regional differences were present between genotypes for both timepoints separately (3 mo: main effect of region $F(3,76) = 45.46$, $p < 0.0001$; main effect of genotype $F(1,76) = 146.2$, $p < 0.0001$; main effect of region x genotype $F(3,76) = 3.970$, $p = 0.0110$ and 9 mo: main effect of region $F(3,68) = 4.756$, $p = 0.0045$; main effect of genotype $F(1,68) = 40.48$, $p < 0.0001$; main effect of region x genotype $F(3,68) = 0.2035$, $p = 0.8936$). For the longitudinal data, a mixed-effects model was used to analyze repeated measures data, thereby allowing two missing observations in the wt group at 9 mo. The model was fitted with genotype (wt and ko) x time (3 mo and 9 mo) as fixed effects and subject as a random effect. In addition, a *post-hoc* Bonferroni multiple comparisons test was performed. All imaging data is represented as the averaged value ± standard error (SE).

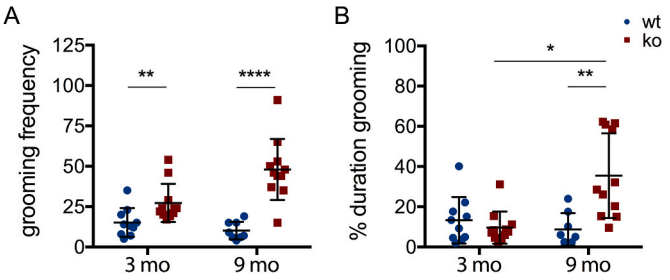

Fig. 1. Progression of compulsive-like grooming in Sapap3 ko mice reflected by the behavioural parameters grooming frequency (A) and % duration grooming (B). The corresponding averaged values can be consulted in Supplementary Table 1. (mo = months; wt = wildtypes; ko = knockouts; *$p < 0.05$, **$p < 0.01$, ****$p < 0.0001$).

A voxel-based analysis was performed on the filtered BP_{ND} images using Statistical Parametric Mapping (SPM) 12 (Wellcome Department of Imaging Neuroscience, UK) in Matlab (R2016a, The Mathworks Inc, USA). Statistical T-maps were calculated at a significance level of $p = 0.01$ and a cluster threshold of 100 voxels. For *in vitro* data, all reported values are reported as the mean ± standard deviation (SD). Cross-sectional analysis was performed comparing genotypes using a Mann-Whitney test.

3. Results

3.1. Aggravation of pathological grooming in Sapap3 ko mice is reflected by an increased total grooming duration and frequency

At the age of 3 mo and prior to the presence of visible skin lesions, ko mice showed a significantly ($p = 0.0050$) higher grooming initiation frequency compared to wt mice (Fig. 1A). There was no significant difference in total grooming duration yet. In 9-mo old mice however, both the grooming frequency ($p < 0.0001$) and the % duration ($p = 0.0018$) were significantly higher in the ko group, when compared to the wt counterparts. Pathological grooming longitudinally worsened for ko mice (Fig. 1B), reflected by a significant increase in % grooming duration (+268.25%; $p = 0.0137$). For the grooming frequency (Fig. 1A), a clear trend was found (+76.02%; $p = 0.0518$). For the wt animals, both parameters remained at similar levels over time.

3.2. Knockout mice show a cross-sectional difference and longitudinal decline in mGluR5 availability for [^{11}C]ABP688

Resulting averaged BP_{ND} images for both groups and at both timepoints are represented in Fig. 2, while Fig. 3 displays the corresponding BP_{ND} values. A cross-sectional comparison between ko and wt mice at the age of 3 mo pinpointed a significantly lower [^{11}C]ABP688 BP_{ND} in ko animals for the cortex (−16.73 ± 3.08%, $p < 0.0001$), the striatum (−20.12 ± 2.43%, $p < 0.0001$), the hippocampus (−18.02 ± 2.64%, $p < 0.0001$), and the amygdala (−11.11 ± 3.07%, $p = 0.0021$). This significant difference in [^{11}C]ABP688 BP_{ND} between both groups persisted at the 9-mo timepoint for the same regions: the cortex

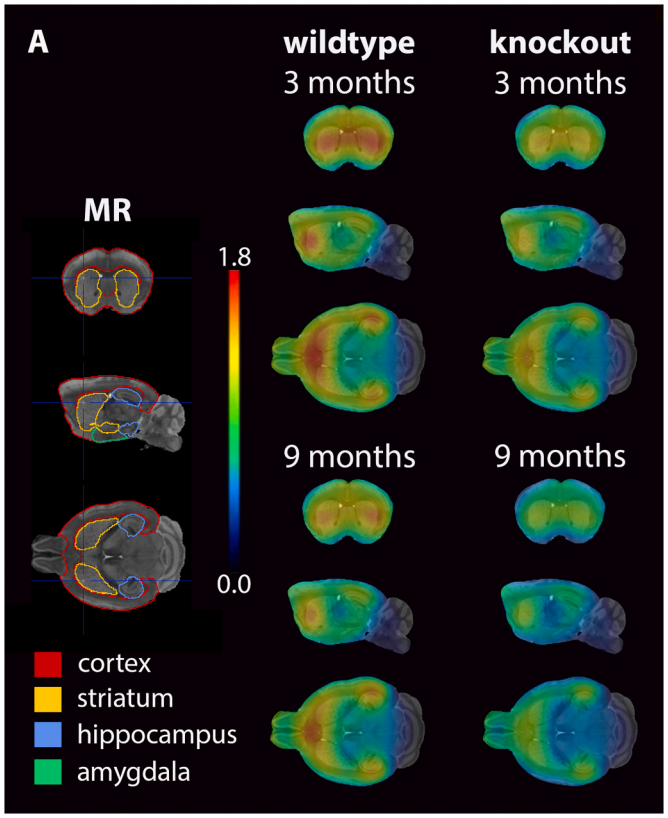

Fig. 2. Averaged [^{11}C]ABP688 BP_{ND} images superimposed on a mouse MR template (delineating cortex, striatum, hippocampus, and amygdala) at both timepoints (3 and 9 mo) and for both groups separately (wt versus ko). For visualization purposes only, an isotropic Gaussian filter (FWHM = 0.5 mm). (MR = magnetic resonance).

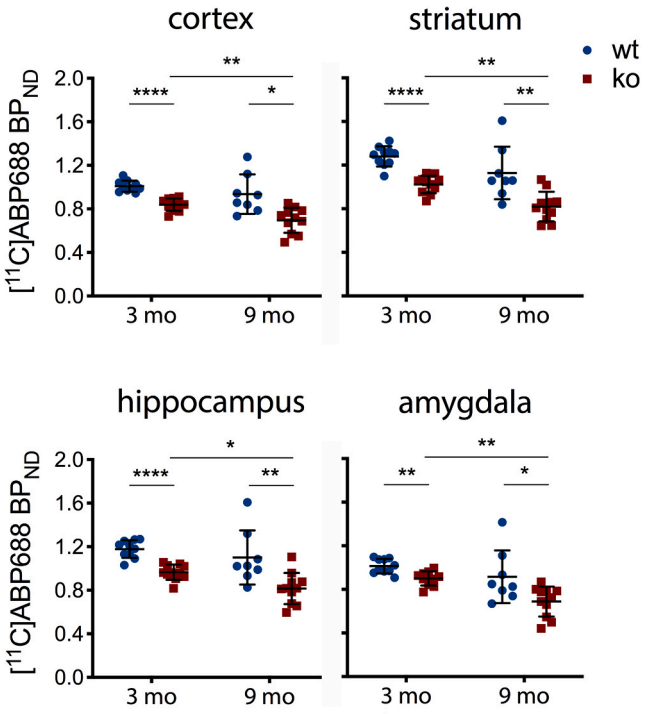

Fig. 3. Averaged BP_{ND} values showing a progressive decline in BP_{ND} in the brain of Sapap3 ko mice in the cortex, the striatum, the hippocampus, and the amygdala. Cross-sectionally, the averaged BP_{ND} value of Sapap3 ko mice is significantly lower in all four regions compared to their wt counterparts both at the age of 3 and 9 mo. The corresponding averaged values can be consulted in Supplementary Table 2. (mo = months; wt = wildtypes; ko = knockouts; *p < 0.05, **p < 0.01, ***p < 0.001, ****p < 0.0001).

(−25.64 ± 8.91%, p = 0.0214), the striatum (−27.30 ± 7.39%, p = 0.0018), the hippocampus (−25.87 ± 7.57%, p = 0.0043), and the amygdala (−24.88 ± 9.09%, p = 0.0318).

For wt animals no significant longitudinal differences were present (Fig. 3). In contrast, ko mice showed a significant temporal BP_{ND} decline in the cortex (−17.14 ± 5.31%, p = 0.0099), the striatum (−19.82 ± 5.58%, p = 0.0049), the hippocampus (−15.53 ± 6.17%, p = 0.0443), and the amygdala (−23.57 ± 6.35%, p = 0.0035).

An additional more sensitive voxel-based analysis confirmed the longitudinal BP_{ND} decline in ko mice. Fig. 4 reveals a significantly lower BP_{ND} in 57.78% of all voxels within the total cortical volume ($p < 0.01$; cluster threshold = 100). This significant BP_{ND} decrease was also present in a substantial part of the voxels from other regions (striatum: 72.15%, hippocampus: 50.27%, and amygdala: 95.54%).

3.3. [^{11}C]ABP688 ex vivo autoradiography supports obtained μPET results

Ex vivo [^{11}C]ABP688 autoradiography of 9 mo old animals showed lower binding in the ko (0.08 %IR/mL) compared the wt (0.14% IR/mL) in the striatum (Fig. 5A). We found parallel results for other measured regions (cortex wt: 0.09 %IR/mL, ko: 0.06 %IR/mL; hippocampus wt: 0.13 %IR/mL, ko: 0.07 %IR/mL). *In vitro* [^{3}H]ABP688 autoradiography, which targets the same mGluR5 binding site, did not confirm *in vivo* findings (Fig. 5B and C). This assay showed no significant differences between both genotypes at the 3 and 9 mo timepoint for the cortex, the striatum, and the hippocampus (Supplementary Table 3).

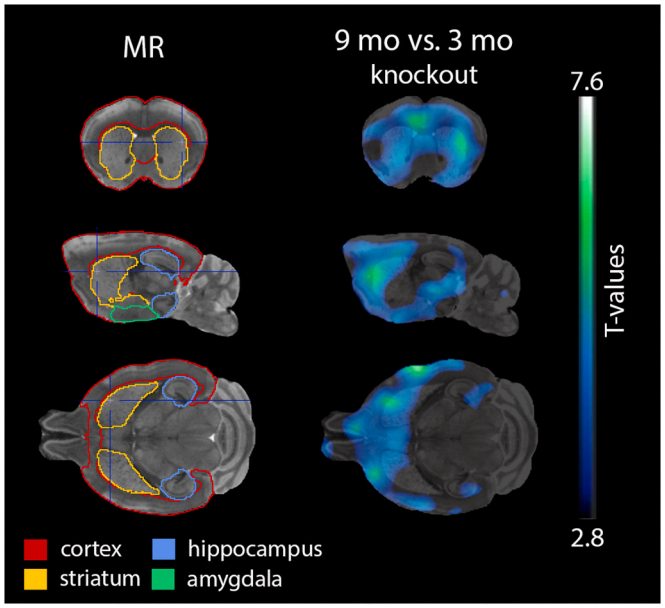

Fig. 4. Hypo T-map (voxel-based SPM analysis) showing clusters of voxels (threshold = 100 voxels) with a significantly ($p < 0.01$) decreased BP_{ND} at 9 mo, when compared to the 3 mo timepoint in Sapap3 ko mice. (ko = knockout; mo = months; MR = magnetic resonance; SPM = statistical parametric mapping).

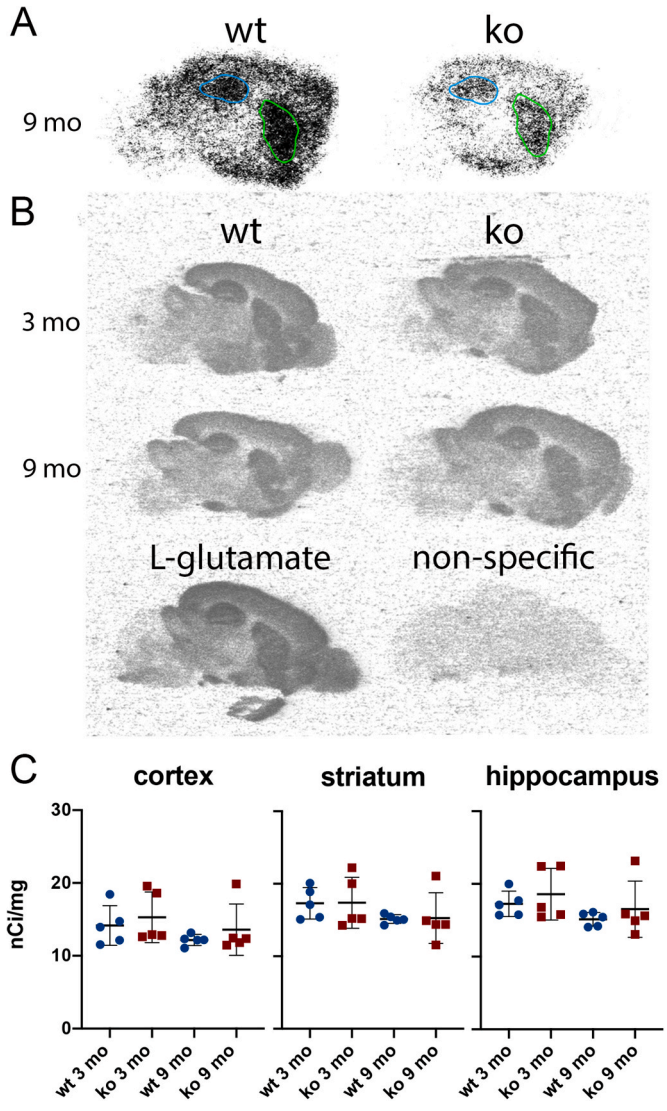

Fig. 5. *Ex vivo* [^{11}C]ABP688 (A) and *in vitro* [^{3}H]ABP688 (B–C) autoradiography with representative raw autoradiograms of sagittal brain sections. The representative images of *ex vivo* autoradiography (A) illustrate the lower [^{11}C]ABP688 binding in the Sapap3 ko brain, in line with the obtained *in vivo* μPET results. The striatum and the hippocampus are delineated in green and blue, respectively. *In vitro* autoradiography (B–C) shows no significant differences in [^{3}H]ABP688 specific binding (nCi/mg) between wt and ko mice for both age groups in the cortex, the striatum, and the hippocampus. As anticipated, the orthosteric ligand L-glutamate did not compete for the allosteric binding site with [^{3}H]ABP688 and the non-specific binding (MTEP + [^{3}H]ABP688) is homogenously distributed throughout the brain. (ko = knockouts; mo = months; wt = wildtypes).

In agreement with *in vitro* [^{3}H]ABP688 autoradiography (Fig. 5B and C), no statistically significant differences were obtained between both genotypes for mGluR5 immunoreactivity in either the cortex (wt: 46.39 ± 13.58%; ko: 57.80 ± 9.55%), the striatum (wt: 68.05 ± 6.47%; ko: 68.41 ± 11.00%), or the hippocampus (wt: 56.25 ± 9.35%; ko: 58.38 ± 12.36%) at the age of 9 mo (Fig. 6).

4. Discussion

To the best of our knowledge, this is the first μPET neuroimaging

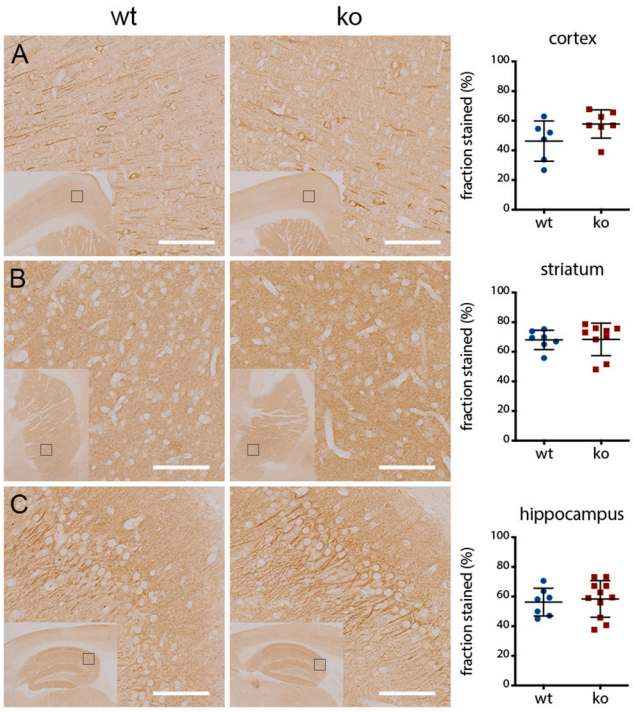

Fig. 6. Representative images of mGluR5 immunoreactivity in 9 mo old animals for the cortex (A), the striatum (B) and the hippocampus (C). No significant differences in % fraction stained were present between genotypes. (ko = knockouts, wt = wildtypes; scale bar 100 μm).

study in a genetic model showing OCD-like behavior. We found a significant progressive decline in allosteric mGluR5 availability ([^{11}C]ABP688 BP_{ND}) in both striatal and extrastriatal regions of Sapap3 ko mice. This decline coincides with an increase in compulsive-like grooming with ageing.

Via a longitudinal evaluation, we found that the grooming frequency is already significantly increased compared to wt controls in 3-mo old Sapap3 ko animals at that time still lacking visible skin lesions. In agreement with previous studies (Welch et al., 2007; Ade et al., 2016; Pinhal, 2018; Xu et al., 2013; van den Boom et al., 2017), 9-mo old Sapap3 ko mice showed significantly increased grooming. Based on the worsening of the phenotype and the role of Sapap3 loss as a driver for mGluR5 alterations underlying OCD-like behavior (Ade et al., 2016; Wan et al., 2011; Chen et al., 2011; Morris et al., 2018), we sought to investigate longitudinal changes in mGluR5 via [^{11}C]ABP688 μPET imaging. *In vivo* regional differences in mGluR5 availability were pinpointed within the corticostriatal axis, which is a key structure in OCD pathophysiology (Harrison et al., 2009, 2013; Fettes et al., 2017) and in the development of OCD-like behavior (Burguière et al., 2015). Indeed, previous studies already established corticostriatal defects in Sapap3 ko mice (Welch et al., 2007; Ade et al., 2016; Corbit et al., 2019; Wan et al., 2014). Two optogenetics studies targeting corticostriatal neurons were able to elicit excessive grooming in wt mice (Ahmari et al., 2013) and alleviate grooming in Sapap3 ko mice (Burguière et al., 2013). Also, striatal deep brain stimulation succeeded to reduce pathological grooming in this model (Pinhal, 2018). Further, we show differences in availability in the hippocampus and the amygdala, which were also suggested to be relevant to OCD beside the well-established CSTC circuit (Milad and Rauch, 2012; Menzies et al., 2008).

Based on previous findings by Ade and colleagues, the origin of the

reduced mGluR5 availability in the Sapap3 ko mouse brain may be explained by the presence of constitutive mGluR5 activation, independent of its orthosteric ligand glutamate (Ade et al., 2016; Ango et al., 2001). Also, other mechanisms for the established [^{11}C]ABP688 BP_{ND} decline in Sapap3 ko mice must be considered. To date no endogenous ligands were described to bind the mGluR5 allosteric site, so an underlying competition phenomenon is unlikely. Another possibility however includes receptor changes, as the BP_{ND} is directly proportional to receptor availability (and possibly expression) and affinity (Innis et al., 2007). G-protein coupled receptors are commonly observed to internalize upon agonist binding and activation (Jong et al., 2018). Namely, glutamate binding could cause the receptor to internalize or to change its affinity at the allosteric site. To date, it is still unknown how glutamate levels impact [^{11}C]ABP688 binding as discussed elsewhere (Smart et al., 2018). Furthermore, a magnetic resonance spectroscopy study found no differences in striatal glutamate content in young adult Sapap3 ko mice (Mintzopoulos et al., 2016). However, receptor internalization could still emerge as an explanation for our findings. Although mGluR5 is activated in absence of glutamate in Sapap3 ko mice, it was previously demonstrated that mGluR5 can also internalize constitutively (Trivedi and Bhattacharyya, 2012).

In line with our *in vitro* regional findings, a Western blot of striatal extracts - using the same antibody as in this study - showed no difference in total striatal mGluR5 levels between wt and ko mice (Ade et al., 2016). Differently, an increased mGluR5 expression was previously demonstrated in Sapap3 ko mice on a neuronal level in cultured striatal medium spiny neurons (Chen et al., 2011). Nevertheless, still a reduced *in vivo* mGluR5 availability was established in brain regions with relevance to OCD-like behavior, which does not seem to result from alterations in overall regional mGluR5 expression levels. Moreover, previous work showed that ABP688 could not access internalized mGluR5 (Lin et al., 2018). As 60–90% of mGluR5 is associated with intracellular structures (Purgert et al., 2014), this could explain why our *in vivo* and *in vitro* findings are not congruent. Presumably, a different pool of receptors is accessible *in vivo* for binding compared to the situation *in vitro* (Elmenhorst et al., 2010) for example with regard to cell membrane integrity. This is also substantiated by the [^{11}C]ABP688 *ex vivo* autoradiography showing lower mGluR5 binding in ko mice confirming the obtained μPET results.

A previous study demonstrated acute alleviation of grooming in Sapap3 ko mice after treatment with the negative allosteric drug MTEP (Ade et al., 2016). Both MTEP and ABP688 target a similar binding site as shown *in vivo* by DeLorenzo and colleagues in baboons (Delorenzo et al., 2011) and as confirmed by our *in vitro* [^{3}H]ABP688 autoradiography MTEP blocking results in mice. Although we established decreased mGluR5 availability with [^{11}C]ABP688, still a therapeutic effect could be achieved with MTEP. Possible explanations include differences in the potency, kinetics, and dosing of these separate ligands. As previously mentioned, *in vivo* [^{11}C]ABP688 binding might be limited to surface receptors, whereas MTEP may target a different pool of mGluR5 *in vivo*. Indeed, it was previously shown that certain ligands targeting mGluR5 do not pass the cell membrane whereas others such as MPEP were able to reach intracellular mGluR5 (Jong et al., 2014).

On a clinical level, the only [^{11}C]ABP688 PET study carried out in OCD patients reported no differences in mGluR5 availability (Akkus et al., 2014). Importantly however, a positive correlation was found between mGluR5 availability and the Y-BOCS obsession subscore. Also in OCD patients, a randomized placebo-controlled phase 2 study with the mGluR5 negative allosteric drug mavoglurant as an add-on treatment for SSRIs was terminated due to a lack of efficacy (Rutrick et al., 2017). Hence, both the decreased mGluR5 availability and allosteric drug effect in Sapap3 ko mice were not supported by human data. As for other psychiatric disorders such as major depressive disorder (Esterlis et al., 2018), preclinical data on mGluR5 in disease models can contrast with findings in human studies. For example, these mice totally lack Sapap3 while patient data suggest more subtle alterations. Beside species differences, this might imply the presence of different underlying pathological mechanisms. Also, this is likely a consequence of the fact that this model is characterized by a repertoire of OCD-"like" behaviors, which does not necessarily represent the situation in patients. In this context, it could be of relevance to reconsider this model as a more general model for repetitive behavior with relevance to a range of disorders such as fragile X syndrome and autism.

For OCD and neuropsychiatric disease in general, the challenge remains to determine which (sub)groups may have mGluR5 abnormalities and could benefit from therapy targeting this receptor. In this context, the aforementioned clinical [^{11}C]ABP688 PET study included patients from different symptom clusters and with different comorbidities and treatment regimens (Akkus et al., 2014). Additionally, mavoglurant was administered in combination with SSRIs which were previously shown to impact the glutamatergic system (Musazzi et al., 2013). Therefore, potential beneficial effects on mGluR5 could be concealed.

Altogether, these findings suggests the presence of a dynamic pathological process related to mGluR5 in the brain of Sapap3 ko mice, with [^{11}C]ABP688 μPET as a potential biomarker. As shown here, *in vitro* mGluR5 data are not necessarily an exact representation of how this receptor behaves *in vivo* and therefore this study proofs the important role of *in vivo* PET in the longitudinal follow-up of receptor systems and their functionality. Also, the worsening of grooming together with the involvement of Sapap3 in synaptic organization (Zhu et al., 2017) underlines the need for a longitudinal assesment of the synaptic density for which a PET marker is readily available (Bertoglio et al., 2019). Despite the current clinical findings in OCD patients, still a growing amount of evidence points towards a role for the glutamatergic system in OCD. Further work is necessary using mGluR5 PET with a strong focus on symptom clusters, comorbidities, and medication history thereby tackling OCD heterogeneity and working towards dimensional psychiatry.

5. Conclusion

Sapap3 ko mice show dynamic alterations in mGluR5 availability in OCD-relevant brain regions with ageing and the progression of OCD-like pathological grooming. This μPET study identified a potential role for [^{11}C]ABP688 as a biomarker for such progression *in vivo* and pinpointed discrepancies between *in vivo* and *in vitro* characterization of mGluR5.

CRediT authorship contribution statement

Dorien Glorie: Conceptualization, Methodology, Validation, Formal analysis, Investigation, Writing - original draft, Visualization. **Jeroen Verhaeghe:** Software, Formal analysis. **Alan Miranda:** Software, Formal analysis. **Istvan Kertesz:** Investigation, Resources. **Leonie wyffels:** Resources, Supervision. **Sigrid Stroobants:** Writing - review & editing. **Steven Staelens:** Conceptualization, Methodology, Writing - review & editing, Supervision, Project administration.

Declaration of competing interest

The authors declare that the research was conducted in the absence

of any commercial or financial relationships that could be construed as a potential conflict of interest.

Acknowledgements

The authors thank Annemie van Eetveldt, Philippe Joye, Caroline Berghmans, and Eleni Van der Hallen of the Molecular Imaging Center Antwerp (MICA) for their important technical support.

Appendix A. Supplementary data

Supplementary data to this article can be found online at https://doi.org/10.1016/j.neuropharm.2020.108160.

Funding

This work was funded by Antwerp University, Belgium through a PhD grant for D. Glorie, a full professor position for S. Staelens and S. Stroobants, and an assistant professor position for J. Verhaeghe and L. wyffels. S. Stroobants is also supported by Antwerp University Hospital, Belgium through a departmental position. Hardware and experimental costs were supported by a DOCPRO (41/FA020000/FFB140317) of the University of Antwerp and an FWO KAN (42/FA020000/685). No funding sources had a role in the study design or in the collection, analysis and interpretation of the data.

References

Abramowitz, J.S., Taylor, S., McKay, D., 2009. Obsessive-compulsive disorder. Lancet 374, 491–499.
Ade, K.K., et al., 2016. Increased metabotropic glutamate receptor 5 signaling underlies obsessive-compulsive disorder-like behavioral and striatal circuit abnormalities in mice. Biol. Psychiatr. 80, 522–533.
Ahmari, S.E., et al., 2013. Repeated cortico-striatal stimulation generates persistent OCD-like behavior. Science 340, 1234–1239.
Akkus, F., et al., 2014. Metabotropic glutamate receptor 5 binding in patients with obsessive-compulsive disorder. Int. J. Neuropsychopharmacol. 17, 1915–1922.
Ametamey, S.M., et al., 2006. Radiosynthesis and preclinical evaluation of 11C-ABP688 as a probe for imaging the metabotropic glutamate receptor subtype 5. J. Nucl. Med. 47, 698–705.
Ango, F., et al., 2001. Agonist-independent activation of metabotropic glutamate receptors by the intracellular protein Homer. Nature 411, 962–965.
Bertoglio, D., et al., 2019. Validation and noninvasive kinetic modeling of [11 C]UCB-J PET imaging in mice. J. Cerebr. Blood Flow Metabol. https://doi.org/10.1177/0271678x19864081.
Bienvenu, O.J., et al., 2009. Sapap3 and pathological grooming in humans: results from the OCD collaborative genetics study. Am. J. Med. Genet. Part B Neuropsychiatr. Genet. https://doi.org/10.1002/ajmg.b.30897.
Burguière, E., Monteiro, P., Feng, G., Graybiel, A.M., 2013. Optogenetic stimulation of lateral orbitofronto-striatal pathway suppresses compulsive behaviors. Science 340, 1243–1246.
Burguière, E., Monteiro, P., Mallet, L., Feng, G., Graybiel, A.M., 2015. Striatal circuits, habits, and implications for obsessive-compulsive disorder. Curr. Opin. Neurobiol. https://doi.org/10.1016/j.conb.2014.08.008.
Chen, M., et al., 2011. Sapap3 deletion anomalously activates short-term endocannabinoid-mediated synaptic plasticity. J. Neurosci. https://doi.org/10.1523/JNEUROSCI.1701-11.2011.
Corbit, V.L., Manning, E.E., Gittis, A.H., Ahmari, S.E., 2019. Strengthened inputs from secondary motor cortex to striatum in a mouse model of compulsive behavior. J. Neurosci. https://doi.org/10.1523/JNEUROSCI.1728-18.2018.
Delorenzo, C., et al., 2011. In vivo positron emission tomography imaging with [11C]ABP688: binding variability and specificity for the metabotropic glutamate receptor subtype 5 in baboons. Eur. J. Nucl. Med. Mol. Imag. https://doi.org/10.1007/s00259-010-1723-7.
Denys, D., et al., 2010. Deep brain stimulation of the nucleus accumbens for treatment-refractory obsessive-compulsive disorder. Arch. Gen. Psychiatr. https://doi.org/10.1001/archgenpsychiatry.2010.122.
Elmenhorst, D., et al., 2010. In vivo and in vitro validation of reference tissue models for the mGluR 5 ligand [11C]ABP688. J. Cerebr. Blood Flow Metabol. https://doi.org/10.1038/jcbfm.2010.65.
Esterlis, I., Holmes, S.E., Sharma, P., Krystal, J.H., DeLorenzo, C., 2018. Metabotropic glutamatergic receptor 5 and stress disorders: knowledge gained from receptor imaging studies. Biol. Psychiatr. https://doi.org/10.1016/j.biopsych.2017.08.025.
Fettes, P., Schulze, L., Downar, J., 2017. Cortico-striatal-thalamic loop circuits of the orbitofrontal cortex: promising therapeutic targets in psychiatric illness. Front. Syst. Neurosci. https://doi.org/10.3389/fnsys.2017.00025.
Graybiel, A.M., Rauch, S.L., 2000. Toward a neurobiology of obsessive-compulsive disorder. Neuron 28, 343–347.
Harrison, B.J., et al., 2009. Altered corticostriatal functional connectivity in obsessive-compulsive disorder. Arch. Gen. Psychiatr. https://doi.org/10.1001/archgenpsychiatry.2009.152.
Harrison, B.J., et al., 2013. Brain corticostriatal systems and the major clinical symptom dimensions of obsessive-compulsive disorder. Biol. Psychiatr. https://doi.org/10.1016/j.biopsych.2012.10.006.
Hume, S.P., Gunn, R.N., Jones, T., 1998. Pharmacological constraints associated with positron emission tomographic scanning of small laboratory animals - Springer. Eur. J. Nucl. Med. 25 (2), 173–176. https://doi.org/10.1007/s002590050211.
Innis, R.B., et al., 2007. Consensus nomenclature for in vivo imaging of reversibly binding radioligands. J. Cereb. Blood Flow Metab. Metab. 27, 1533–1539.
Johnson, G.A., et al., 2010. Waxholm Space: an Image-Based Reference for Coordinating Mouse Brain Research. Neuroimage. https://doi.org/10.1016/j.neuroimage.2010.06.067.
Jong, Y.J.I., Sergin, I., Purgert, C.A., O'Malley, K.L., 2014. Location-dependent signaling of the group 1 metabotropic glutamate receptor mGlu5. Mol. Pharmacol. https://doi.org/10.1124/mol.114.094763.
Jong, Y.J.I., Harmon, S.K., O'Malley, K.L., 2018. Intracellular GPCRs play key roles in synaptic plasticity. ACS Chem. Neurosci. https://doi.org/10.1021/acschemneuro.7b00516.
Lammertsma, A.A., Hume, S.P., 1996. Simplified reference tissue model for PET receptor studies. Hum. Brain Mapp. J. 4, 153–158.
Lin, X., Donthamsetti, P., Skinberg, M., Slifstein, M., Abi-Dargham, A., Javitch, J., 2018. FPEB and ABP688 Cannot Accesss Internalized mGluR5 Receptors.
Mahgoub, M., et al., 2016. MeCP2 and histone deacetylases 1 and 2 in dorsal striatum collectively suppress repetitive behaviors. Nat. Neurosci. 19, 1506–1512.
Menzies, L., et al., 2008. Integrating evidence from neuroimaging and neuropsychological studies of obsessive-compulsive disorder: the orbitofronto-striatal model revisited. Neurosci. Biobehav. Rev. 32, 525–549.
Milad, M.R., Rauch, S.L., 2012. Obsessive-compulsive disorder: beyond segregated cortico-striatal pathways. Trends Cognit. Sci. 16, 43–51.
Mintzopoulos, D., et al., 2016. Striatal magnetic resonance spectroscopy abnormalities in young adult SAPAP3 knockout mice. Biol. psychiatry Cogn. Neurosci. neuroimaging 1, 39–48.
Morris, C.W., Watkins, D.S., Salek, A.B., Edler, M.C., Baucum, A.J., 2018. The association of spinophilin with disks large-associated protein 3 (SAPAP3) is regulated by metabotropic glutamate receptor (mGluR) 5. Mol. Cell. Neurosci. 90, 60–69.
Murray, C.J., Lopez, A., 1996. A comprehensive assessment of mortality and disability from disease, injures and risk factors in 1990 and projected to 2020. The Global Burden of Disease. https://doi.org/10.1186/1471-2458-13-863.
Musazzi, L., Treccani, G., Mallei, A., Popoli, M., 2013. The action of antidepressants on the glutamate system: regulation of glutamate release and glutamate receptors. Biol. Psychiatr. https://doi.org/10.1016/j.biopsych.2012.11.009.
O'Connor, E.C., Bariselli, S., Bellone, C., 2014. Synaptic basis of social dysfunction: a focus on postsynaptic proteins linking group-I mGluRs with AMPARs and NMDARs. Eur. J. Neurosci. https://doi.org/10.1111/ejn.12510.
Pack, A.I., et al., 2007. Novel method for high-throughput phenotyping of sleep in mice. Physiol. Genom. https://doi.org/10.1152/physiolgenomics.00139.2006.
Pauls, D.L., Abramovitch, A., Rauch, S.L., Geller, D.A., 2014. Obsessive-compulsive disorder: an integrative genetic and neurobiological perspective. Nat. Rev. Neurosci. 15, 410–424.
Piantadosi, S.C., Chamberlain, B.L., Glausier, J.R., Lewis, D.A., Ahmari, S.E., 2019. Lower excitatory synaptic gene expression in orbitofrontal cortex and striatum in an initial study of subjects with obsessive compulsive disorder. Mol. Psychiatr. https://doi.org/10.1038/s41380-019-0431-3.
Pinhal, C.M., et al., 2018. Differential effects of deep brain stimulation of the internal capsule and the striatum on excessive grooming in Sapap3 mutant mice. Biol. Psychiatr. 84 (12), 917–925. https://doi.org/10.1016/j.biopsych.2018.05.011.
Purgert, C.A., et al., 2014. Intracellular mGluR5 can mediate synaptic plasticity in the hippocampus. J. Neurosci. https://doi.org/10.1523/JNEUROSCI.3451-13.2014.
Ruscio, A.M., Stein, D.J., Chiu, W.T., Kessler, R.C., 2010. The epidemiology of obsessive-compulsive disorder in the national comorbidity survey replication. Mol. Psychiatr. https://doi.org/10.1038/mp.2008.94.
Rutrick, D., et al., 2017. Mavoglurant augmentation in OCD patients resistant to selective serotonin reuptake inhibitors: a proof-of-concept, randomized, placebo-controlled, phase 2 study. Adv. Ther. https://doi.org/10.1007/s12325-016-0468-5.
Smart, K., et al., 2018. Test–retest variability of [11 C]ABP688 estimates of metabotropic glutamate receptor subtype 5 availability in humans. Synapse. https://doi.org/10.1002/syn.22041.
Stewart, S.E., et al., 2013. Genome-wide association study of obsessive-compulsive disorder. Mol. Psychiatr. https://doi.org/10.1038/mp.2012.85.
Ting, J.T., Feng, G., 2011. Neurobiology of obsessive-compulsive disorder: insights into neural circuitry dysfunction through mouse genetics. Curr. Opin. Neurobiol. 21, 842–848.
Trivedi, R.R., Bhattacharyya, S., 2012. Constitutive internalization and recycling of

metabotropic glutamate receptor 5 (mGluR5). Biochem. Biophys. Res. Commun. https://doi.org/10.1016/j.bbrc.2012.09.040.
van den Boom, B.J.G., Pavlidi, P., Wolf, C.J.H., Mooij, A.H., Willuhn, I., 2017. Automated classification of self-grooming in mice using open-source software. J. Neurosci. Methods 289, 48–56.
Verhaeghe, J., et al., 2018. Noninvasive relative quantification of [11C]ABP688 PET imaging in mice versus an input function measured over an arteriovenous shunt. Front. Neurol. https://doi.org/10.3389/fneur.2018.00516.
Wan, Y., Feng, G., Calakos, N., 2011. Sapap3 deletion causes mGluR5-dependent silencing of AMPAR synapses. J. Neurosci. https://doi.org/10.1523/JNEUROSCI.2533-11.2011.
Wan, Y., et al., 2014. Circuit-selective striatal synaptic dysfunction in the Sapap3 knockout mouse model of obsessive-compulsive disorder. Biol. Psychiatr. 75, 623–630.
Welch, J.M., et al., 2007. Cortico-striatal synaptic defects and OCD-like behaviours in Sapap3-mutant mice. Nature. https://doi.org/10.1038/nature06104.
Wu, Y., Carson, R.E., 2002. Noise reduction in the simplified reference tissue model for neuroreceptor functional imaging. J. Cerebr. Blood Flow Metabol. https://doi.org/10.1097/01.WCB.0000033967.83623.34.
Xu, P., et al., 2013. Double deletion of melanocortin 4 receptors and SAPAP3 corrects compulsive behavior and obesity in mice. Proc. Natl. Acad. Sci. U.S.A. 110, 10759–10764.
Zhu, J., et al., 2017. Synaptic targeting and function of SAPAPs mediated by phosphorylation-dependent binding to PSD-95 MAGUKs. Cell Rep. https://doi.org/10.1016/j.celrep.2017.11.107.
Züchner, S., et al., 2009. Multiple rare SAPAP3 missense variants in trichotillomania and OCD. Mol. Psychiatr. https://doi.org/10.1038/mp.2008.83.